Asian Journal of Chemistry; Vol. 35, No. 6 (2023), 1525-1532

ASIAN JOURNAL OF CHEMISTRY

https://doi.org/10.14233/ajchem.2023.27625

Role of Annealing Temperature in Tuning Magnetic Properties of Fe-Co-Al_2O_4 Spinel Aluminates

R. POONGODI[1], S. SENGUTTUVAN[1,*] and R. SAGAYARAJ[2,*]

[1]PG & Research Department of Chemistry, Thiru.Vi.Ka. Government Arts College (Affiliated to Bharathidasan University), Thiruvarur-610003, India

[2]PG & Research Department of Physics, St. Joseph's College of Arts and Science (Autonomous) (Affiliated to Annamalai University), Cuddalore-607001, India

*Corresponding authors: E-mail: senguttuvanathan@gmail.com; sagayarajnancy@gmail.com

Received: 10 February 2023; *Accepted*: 12 May 2023; *Published online*: 27 May 2023; AJC-21272

The annealing temperature (600, 700, 800, 900, 1000 ºC) can have a significant effect on the microstructure, surface functionalization, surface morphology and magnetic properties of the Fe-Co-Al_2O_4 spinel aluminates synthesized by the coprecipitation method. Increasing the annealing temperature leads to a change in the crystalline structure of the spinel aluminates, resulting in different physical and magnetic properties. By controlling the annealing temperature, it is possible to obtain improved structural stability, higher crystallinity and better magnetic properties of the Fe-Co-Al_2O_4 spinel aluminates. The annealing temperature also affects the microstructure and morphology of the spinel aluminates, resulting in different XRD patterns, FTIR spectra and FE-SEM images. As a result, affects the crystallite size (D: 9.49 to 14.25 nm), lattice constant (a: 8.1506 to 8.2889 Å) and surface area of the spinel aluminates, resulting in different anisotropy constant (K: 33.06 to 66.48 J/m^3) values. The VSM study showed that higher annealing temperatures have a positive effect on the magnetic properties of Fe-Co-Al_2O_4 samples. The increased magnetization capacity of these samples can be attributed to the multi-domain nature of their crystallites, which allows for better magnetic moment ordering and improved magnetization performance (M_s: 45.421 × 10^{-3} to 0.13635 emu/g). At higher temperatures, more atoms were able to move and reorient themselves, resulting in higher coercivity (H_c: 391.75 to 873.02 Oe), magnetic moment (μB: 0.0029 to 0.007 μB Tesla) and Remnant ratio (R: 0.4113 to 0.4570 no unit) values.

Keywords: Annealing temperature, Coercivity, Magnetization, Coprecipitation, Spinel aluminates, Magnetic properties.

INTRODUCTION

A spinel is a type of crystal structure characterized by the general chemical formula AB_2O_4 in which A indicates a divalent cation, B a trivalent cation and O a divalent anion. This formula consists of two types of cations: divalent A^{2+} cation such as nickel, magnesium, zinc, cadmium, manganese and a trivalent B^{3+} cation such as aluminum, indium, vanadium, iron, titanium, *etc*. The spinel unit cell is an arrangement of 8 face-centered cubic (FCC) cells, with a total of four oxide ions positioned at the FCC lattice points. The divalent A^{2+} cations occupy one eighth (1/8th) of the tetrahedral voids, while the trivalent B^{3+} cations occupy half (1/2) of the octahedral voids. This creates a compound with the formula $(A^{2+})_{tet}(B^{3+})_{2oct}O_4$. Normal spinels, such as $MgAl_2O_4$, $FeAl_2O_4$ and $ZnAl_2O_4$, are composed of AB_2O_4 that have applications in various areas like magnetic materials, ceramics and catalysis [1-6]. Inverse spinels, on the other hand, contain the general structure $B(AB)O_4$, where, the A^{2+} cations occupy the octahedral voids, while half of the B^{3+} cations occupy the tetrahedral and the other half occupy the octahedral sites. This arrangement can be expressed as $(B^{3+})_{tet}(A^{2+}B^{3+})_{oct}O_4$ and the examples of inverse spinels include Fe_3O_4, $MgFe_2O_4$ and $MnFe_2O_4$ [7-9].

Spinel aluminates are an inorganic compound consisting of aluminum, oxygen and one or more other metal ions. It is found in nature as spinels and synthetic forms and is used in a variety of industrial applications. It has a wide range of applications including catalysts, pigments, ceramic glazes and polishing compounds. The chemical composition of spinel aluminates includes two components. The first component, Al_2O_3 is responsible for the material's powdery texture and high melting point. The second component, generally a metallic ion like Fe, Co, Ti or Ni, contributes to its colour and structural properties. Spinel aluminates have several characteristics that make it an attractive

material for a wide range of applications. It is highly heat and corrosion resistant, making it ideal for coating metals and other surfaces. Furthermore, the material is non-toxic and relatively low in cost. In addition, the abundance of raw materials used to produce spinel aluminates makes it readily available and cost-effective [4,10,11]. $CoAl_2O_4$ is a type of inverse spinel, which can have random or defected structures. This is due to the fact that cobalt ions have a greater preference for octahedral sites rather than tetrahedral sites. On the other hand, aluminum ions also have a strong affinity for octahedral sites due to their high lattice energy. As a result, the cations are almost completely randomized on all available sites, resulting in the formula $(Al_{0.75}Co_{0.25})_{tet}[Co_{0.75}Al_{1.25}]_{octa}O_4$. This randomization effectively creates a mixture of Co^{2+} and Al^{3+} ions on both octahedral and tetrahedral sites, leading to a crystal structure that is neither completely random nor completely defected. This unique composition of ions creates a wider range of properties and applications for $CoAl_2O_4$ compared to more traditional spinel structures [12-18]. The relative sizes of A and B cations in spinels are an important factor in determining the crystal structure. In general, the smaller cation has a preference for the site of lower coordination, namely the tetrahedral site. However, in case of $MgAl_2O_4$, the lattice energy of the smaller cation, Al^{3+}, is greater than that of the larger cation, Mg^{2+}. This leads to the Al^{3+} occupying the octahedral sites, resulting in a normal spinel structure. If this weren't the case, then the "spinel" would have an inverse spinel structure. Additionally, when the relative sizes of A and B cations are different, it can lead to randomization of all cations on available sites, creating structures with unique compositions and properties [19-22].

Many researchers have studied the effects of substituting magnetic and non-magnetic cations on the magnetic properties of cobalt ferrite. Spinel ferrites possess a unique combination of physical and chemical properties due to their capacity to distribute cations amongst the tetrahedral (A) and octahedral sites (B). This allows for the manipulation of the magnetic properties of compound [23]. The presence of non-magnetic Al^{3+} cations in cobalt ferrite increases the lattice constant and decreases the grain size, leading to a decrease in the saturation magnetization (M_s) and coercivity (H_c). This is due to the weakening of the interaction between sublattices caused by the addition of non-magnetic Al^{3+} ions [24]. Waghmare *et al.* [24] suggested that the decrease in magnetization caused by the increase of Al^{3+} content can be attributed to cation distribution between tetrahedral (A) and octahedral (B) sites. The substitution of non-magnetic Al^{3+} ions for Fe^{3+} ions causes them to occupy the octahedral site instead of the tetrahedral site, weakening the A-B interaction. This is due to the non-magnetic nature of the Al^{3+} ions, which prevents them from taking part in the exchange interaction. Therefore, the saturation magnetization decreases with an increase of Al^{3+} content. Yakovlev *et al.* [25] suggested that the coercivity decreases with an increase of Al^{3+} ion concentration due to the decrease in anisotropy field, which in turn decreases the domain wall energy.

The $CoAl_2O_4$ compound contains Al^{3+} and Co^{2+} ions, which are replaced by –OH or –COOH ligands in the solution. This creates a single molecule unit of metal complexonate containing one Co^{2+} ion, two Al^{3+} ions and four complexonate anions. Exposure to ^{60}Co γ-source at room temperature produces an energy stabilized gel [15]. The $CoAl_2O_4$ spinel used in cobalt blue pigments is usually manufactured by a solid-state reaction process using cobalt oxide and alumina as the raw materials. This process takes place at high temperatures (1200-1300 ºC) [26]. It can be seen that the intensity of $CoAl_2O_4$ spinel phase increases with increasing Co/Al mole ratio. Since, the $CoAl_2O_4$ spinel phase is the main factor in creating blue hues for the blue pigments, this is beneficial for producing vibrant blue hues in hybrid pigments. The intensity of Al_2O_3 diffraction peaks decreases with an increase of the Co/Al mole ratio, indicating that more Al^{3+} ions are reacting with Co^{2+} to form $CoAl_2O_4$, results in a thicker $CoAl_2O_4$ shell layer and, consequently, a lower relative proportion of Al_2O_3 in the hybrid pigments [11]. Pure $CoAl_2O_4$ pigment ($2\theta = 37.0496^o$) can be obtained above 800 ºC [13]. Three characteristic absorption bands of cobalt blue pigments at around 547, 584 and 624 nm are observed, which correspond to the spin-allowed transitions of Co^{2+} ions in the visible region. The blue colour of the hybrid pigments is the complementary colour due to the light absorption in this range. As the cobalt content of the hybrid pigments increases, the observed absorption bands become more intense, resulting in a more vibrant blue colour of the pigments [11].

The $CoAl_2O_4$ ceramic pigments have a low chroma value, which can negatively affect the stability and quality of ceramic glazing, enamel glazing and ceramic product printing. The colouration mechanism and colour stability of $CoAl_2O_4$ ceramic pigments after high-temperature sintering are significant factors and the Co content, Co ion valence and coordination number all influence the pigments. Furthermore, during the coating sintering process, de-oxidation reactions can convert Co^{3+} into Co^{2+}, which increases the chroma of blue $CoAl_2O_4$ pigments [12]. An increase in the Co content decreases the number of Al^{3+} ions in the tetrahedron, which leads to the formation of Co^{3+} or excess Co^{2+} ions that occupy the octahedral interstices. This structural difference results in a change in splitting energy of ligand field and ultimately, a colour change of the ceramic pigments [12]. Blue $CoAl_2O_4$ pigment is an inorganic pigment that is used for a variety of purposes. This pigment is resistant to acid and alkali and has increased thermal stability, making it ideal for use in plastics colouring, paints, glasses, glazes and porcelain enamels [16]. Cobalt aluminate ($CoAl_2O_4$) spinel, more commonly known as Thenard's blue, is a widely used material, possessing numerous properties and applications. It is often used as a catalyst, pigment layer on luminescent materials and colour filter for automotive lamps due to its excellent stability and longevity. Additionally, it has been shown to possess antifouling and antibacterial properties, making it an ideal choice for use in many industries [27]. $CoAl_2O_4$ ceramic pigments have superior performance in terms of thermal stability and chemical stability, making them an ideal choice for many industries. They possess excellent hiding power, colour strength, dispersion, impermeability, non-migration and compatibility with most thermoplastic or thermosetting plastics products. These properties make them widely used in a number of fields, including automotive lamps, plastics colouring, paints, glasses,

glazes and porcelain enamels [28]. This method of preparing $CoAl_2O_4$ ceramic pigments is highly advantageous over the traditional sintering method, as it not only reduces the preparation temperature and time requirements, but also improves the purity of the pigment. It is a more effective method that yields higher quality results, making it a more desirable choice for many industries [29]. The calcination temperature of $CoAl_2O_4$ ceramic pigments has a significant impact on their stability, consistency and particle size. Increasing the calcination temperature to 1000 ºC is beneficial for a complete reaction as well as improved stability; however it does lead to increased energy consumption and larger grain size. The particle size of these pigments was observed to be approximately 30-100 nm at this temperature [30].

Fe-$CoAl_2O_4$ is used in a variety of applications, including catalysts, pigments, ceramic glazes and polishing compounds. Fe- $CoAl_2O_4$is notable for its durability and heat resistance, making it an ideal choice for a variety of industrial and commercial applications. The compound's composition also gives it excellent thermal shock and corrosion resistance, which makes it a great choice for coating and protecting metals [31,32]. Here are five reasons why Fe-$CoAl_2O_4$ is a great choice for industrial and commercial applications for example, durable and heat resistant material, excellent thermal shock and corrosion resistance, effective at coating and protecting metals, non-toxic and relatively low in price, abundant raw materials availability [33,34]. By varying the temperature of an annealing process, the structural, spectroscopic and magnetic properties of Fe-$CoAl_2O_4$ are affected. This research focuses on understanding the relationship between the thermal process and the various physical and chemical characteristics of the material, as well as how these characteristics can affect its overall performance. Upon annealing, the Fe-$CoAl_2O_4$ matrix forms various crystalline structures, depending on the annealing temperature. Tetrahedral sites form cubic structures, while octahedral sites form hexagonal structures. By changing the annealing temperature, different crystalline arrangements can be created and this can have an effect on the physical and chemical properties of the material, such as its electrical conductivity, thermal conductivity and magnetic properties. The high-frequency band at 533.68 cm^{-1} shows the stretching vibrations of tetrahedral groups, while the lower frequency band near 406.01 cm^{-1} indicates the stretching mode of octahedral M-O groups in ferrites. This difference in frequency is due to the different distances between Fe^{3+} ions in octahedral and tetrahedral complexes. A higher level of accuracy can be obtained by analysis of the data on a more precise scale [35]. The aim of this work was to synthesize nanoparticles of Fe-$CoAl_2O_4$ using a coprecipitation method. This technique offers the advantage of controlling size and homogeneity of crystallite size, which can have an impact on the structure and magnetic properties of $CoAl_2O_4$ as well as its colouring ability. Structural confirmation was performed through X-ray diffraction and vibrational phonon modes were studied using Raman spectroscopy. Using a coprecipitation method is beneficial in that it helps to save time and energy.

EXPERIMENTAL

The coprecipitation method was used to separate and purify a desired metal from a solution. By adding a precipitating agent, the metal is caused to form a solid precipitate, which can then be separated from the solution. This approach is relatively simple and economical in comparison to other separation methods and does not require expensive equipment or chemicals. The PVP coated Fe-Co-Al_2O_4 spinel aluminates nanoparticles were synthesized using the co-precipitation procedure. The stoichiometric solutions of aluminum oxide, ferric sulfate, cobalt sulfate, aluminum oxide and polyvinyl pyrrolidone (PVP) were combined and stirred for 3 h at room temperature. During the 3 h stirring period, ammonia solution was added dropwise with stirring which caused the mixture to turn black. The mixture was then maintained at pH 11 in order to create a high electron capture surface and the precipitates were washed three-times in both distilled water and ethanol to remove amine molecules and impurities. Finally, the sample was dried in a hot air oven at 100 ºC for 6 h and annealed by placing it in a muffle furnace at various temperatures (600, 700, 800, 900, 1000 ºC) for 6 h. The resulting Fe-Co-Al_2O_4 spinel aluminates nanoparticles were then collected for further use.

RESULTS AND DISCUSSION

XRD studies: The crystalline structure of the prepared Fe-Co-Al_2O_4 spinel aluminates materials was analyzed by XRD with diffraction angle (2θ) between 20º and 80º. Fig. 1 shows the microstructure of Fe-Co-Al_2O_4 spinel aluminates annealed at 600, 700, 800, 900 and 1000 ºC for 6 h. It reveals that the diffraction peaks would shift to higher angles with increasing temperature. This is because crystal lattices expand as the temperature increases, which causes the diffraction peaks to shift. Different diffraction peaks are observed for the microstructure and peaks are well matched that of spinel cubic and confirmed by JCPDS#07-0068 ($FeAl_2O_4$), JCPDS#89-4308(Co), JCPDS#65-3107 (Fe_3O_4). These peaks elucidated cobalt aluminates phase formation. When the annealing temperature is increased, this leads to greater crystallinity and nanosize, which in turn causes a full width at half maximum (FWHM) of diffraction peaks [36]. The absence of other material or element related peaks indicates that the firing temperature was sufficient to synthesize Fe-Co-Al_2O_4 due to the high temperatures. High temperatures can remove impurities and promote the formation of a homogenous material with desired properties. Strong and wide diffraction peaks indicate that the material was well crystallized because they are a sign of good crystal structure and low crystallite sizes. The crystalline structure of the material forms during the synthesis process and the crystallite sizes influence how much energy is needed to produce the diffraction peak, which results in a stronger and wider peak [35,37]. The higher annealing temperature causes the ions to move faster, which allows them to interact more and form a more organized crystalline structure. This improved arrangement of ions increases the intensity of diffraction peaks at the (311) position because the arrangement of ions is more consistent and the crystallite size is smaller. The smaller size results in a stronger peak when energy is applied [13]. The most intense peak appeared at 2θ = 35.96º for 600 ºC, 2θ = 35.92º for 700 ºC, 2θ = 36.14º for 800 ºC, 2θ = 36.17º for 900 ºC, 2θ = 36.57º for 1000 ºC, which suggested a cubic spinel ferrite

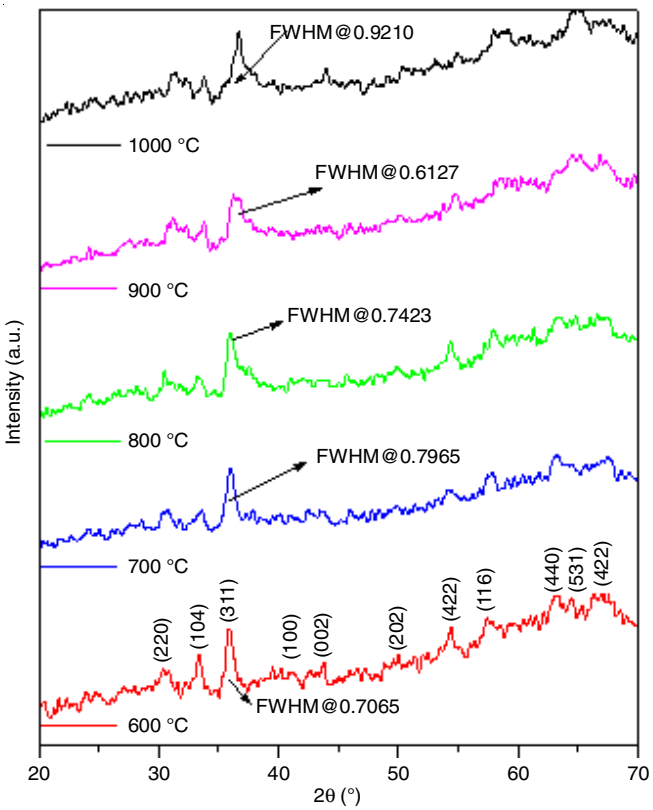

Fig. 1. X-ray diffraction patterns of Fe-Co-Al_2O_4 spinel aluminates annealed at 600, 700, 800, 900 and 1000 °C

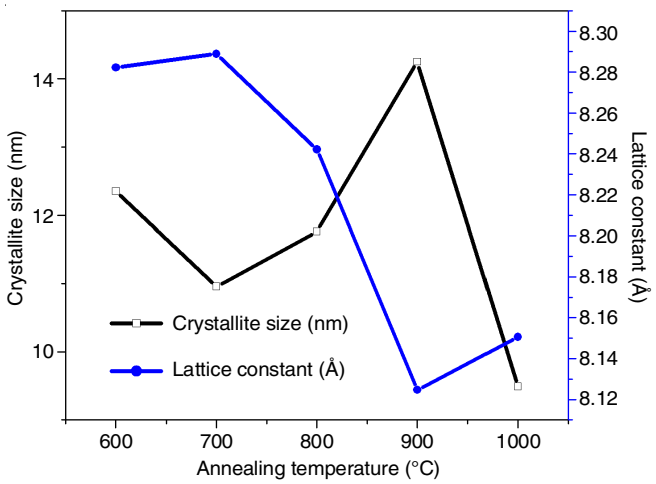

Fig. 2. Relation between crystallite sizes, lattice constant with annealing temperature of Fe-Co-Al_2O_4 spinel aluminates

structure. According to the Debye-Scherrer's formula, the average crystallite size of 600 ºC was 12.35 nm, 10.96 nm for 700 ºC, 11.76 nm for 800 ºC, 14.25 nm for 900 ºC, 9.49 nm for 1000 ºC as shown in Table-1. An increase in lattice constant and crystallite size with rising temperature elucidates that higher temperatures allow for more effective diffusion of ions, leading to more organized and well-defined crystal structures (Fig. 2). The larger Fe^{3+} (0.67 Å) atoms are replaced by smaller Al^{3+} (0.51 Å) atoms, thus decreasing the lattice constant from 8.2822 Å to 8.1506 Å. However, this effect is reversed as the sintering temperature increases, resulting in an increase in both crystallite size and lattice constant up to 900 ºC. At 1000 ºC, the lattice constant and size further decrease because the high temperature allows for more effective diffusion of atoms and ions, resulting in a more organized crystal structure with smaller crystallite sizes (9.49 nm). The high temperature also causes atoms to more forcefully interact with each other, thus reducing the lattice constant (8.1506 Å). In Fe-Co-Al_2O_4, there is a slight inversion between Co^{2+} and Al^{3+} ions because at higher temperatures (1000 ºC), aluminum ions have more energy to overcome the strong ionic bonds with iron, allowing them to occupy octahedral sites which are energetically favourable [15]. Cobalt on the other hand, due to its smaller size (9.49 nm), does not have enough energy to displace the iron ions and thus opts for the tetrahedral sites [38].

FTIR studies: Fourier transforms infrared (FTIR) spectroscopy can be used to analyze the surface functionalization of Fe-$CoAl_2O_4$ as shown in Fig. 3. The distinct peaks values at 3610-3418 cm^{-1} is due to the O–H vibrations in Fe-Co-Al_2O_4 [39], while the peak at 2339-2072 cm^{-1} is associated with the stretching and bending of bonds of molecules like water, hydrocarbons and alcohols [35]. Additionally, FTIR reveals that Fe-Co-Al_2O_4 contains tetrahedral and octahedral sites, respectively to peaks at 451-364 cm^{-1} and 555-489 cm^{-1}, respectively. In the spinel Fe-Co-Al_2O_4, the absorption band at 451-364 cm^{-1} indicates the presence of Co-O-Al stretching frequencies. This indicates that there is an interaction between cobalt, oxygen and aluminum molecules in the material. Additionally, the band at 555-489 cm^{-1} range belongs to Al-O-Fe vibrations with octahedral sites. These two sites provide useful insights into the material properties of Fe-Co-Al_2O_4 [13,15,16,38].

Raman studies: Fig. 4 shows the vibrational study of iron incorporated cobalt aluminates at room temperature, depicting the phonon vibrational modes in an inverse spinel structure with frequencies ranging from 2000 to 300 cm^{-1}. This type of analysis is used to gain a better understanding of the material's properties and can be used to inform further research [40]. This peak positions and intensities are slightly different until 1000 ºC. In particular, the Co^{2+}/Al-O_4 tetrahedron translation is noticeable between 363-209 cm^{-1} [41,42]. The peak found at 417 cm^{-1} in the Raman spectra of Fe-$CoAl_2O_4$ ceramics is assigned to the symmetric bending motion of oxygen atoms

TABLE-1
STRUCTURAL PARAMETERS OF $Fe_{0.5}Co_{0.5}Al_2O_4$

Sample	2θ	d-spacing	FWHM	Crystallite size (D)	Lattice constant (a)	Strain (ε)
$Fe_{0.5}Co_{0.5}Al_2O_4$/600 °C	35.96	2.4972	0.7065	12.35	8.2822	0.0095
$Fe_{0.5}Co_{0.5}Al_2O_4$/700 °C	35.93	2.4992	0.7965	10.96	8.2889	0.0107
$Fe_{0.5}Co_{0.5}Al_2O_4$/800 °C	36.14	2.4851	0.7423	11.76	8.2421	0.0099
$Fe_{0.5}Co_{0.5}Al_2O_4$/900 °C	36.17	2.4497	0.6127	14.25	8.1247	0.0081
$Fe_{0.5}Co_{0.5}Al_2O_4$/1000 °C	36.57	2.4575	0.9210	9.49	8.1506	0.0121

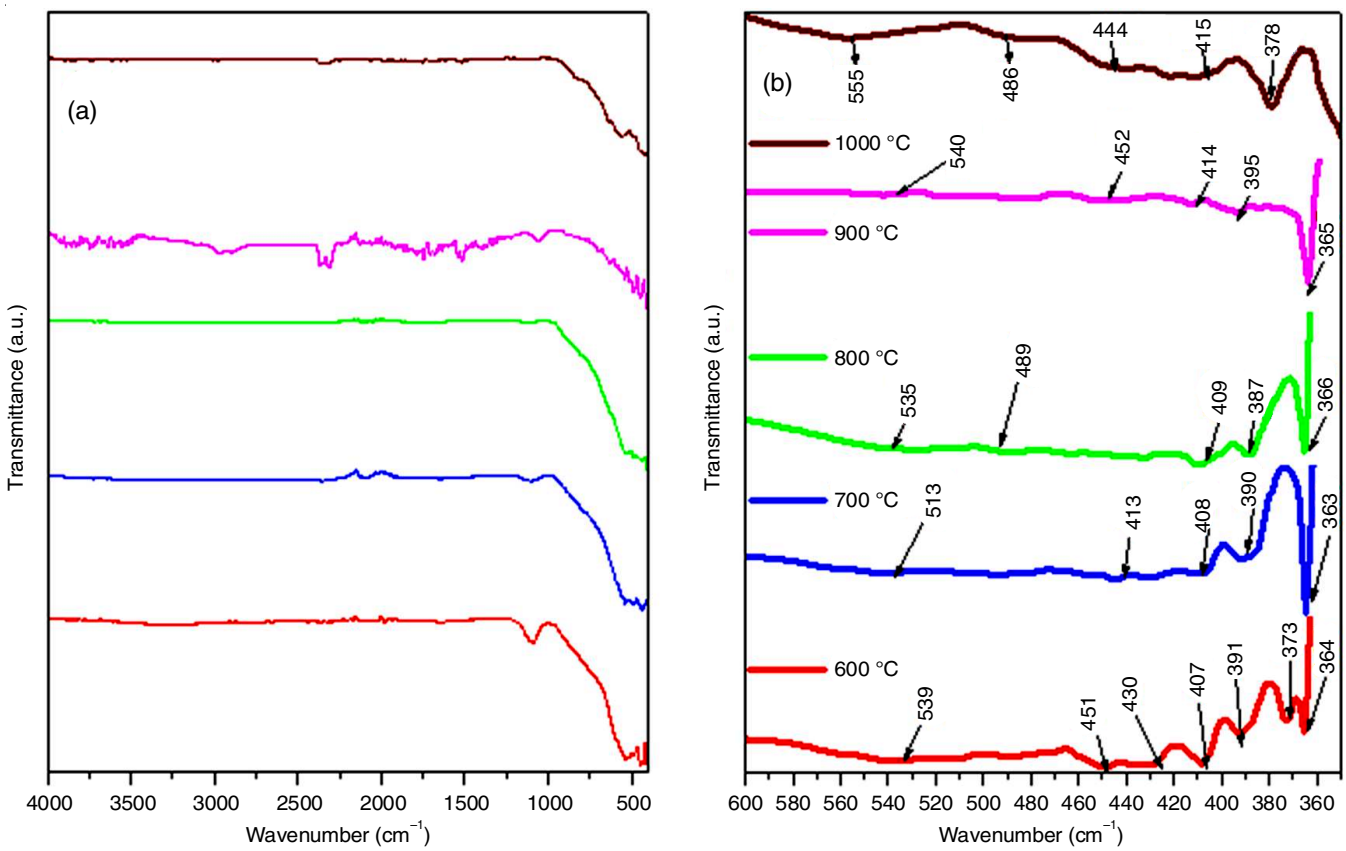

Fig. 3. FTIR spectra (a) not enlarged (b) enlarged of Fe-Co-Al_2O_4 spinel aluminates annealed at 600, 700, 800, 900 and 1000 °C

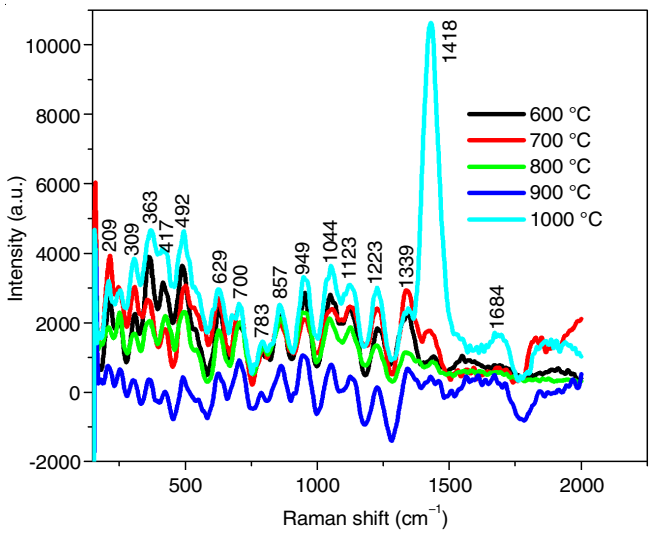

Fig. 4. FT-Raman spectra of Fe-Co-Al_2O_4 spinel aluminates annealed at 600, 700, 800, 900 and 1000 °C

within the tetrahedral structure [43-45]. The vibration frequency found at 492 cm^{-1} in the Raman spectra of Fe-$CoAl_2O_4$ ceramics is due to the asymmetric stretching vibration of Co^{2+}/Al-O in the tetrahedral sites. This motion occurs when the oxygen atoms interact with the tetrahedral cations, resulting in a distinct vibration frequency specific to this structure [41,43,46,47]. There is some debate regarding the vibration assignment at 629 cm^{-1} in the Raman spectra of Fe-$CoAl_2O_4$ ceramics. It has been reported to be either an anti-symmetric stretching mode of the tetrahedron unit or an asymmetric bending motion of the oxygen bonded to the tetrahedral cation [44,47]. Studies on the wavenumber of $A1^{3+}$ mode in Fe-$CoAl_2O_4$ ceramics have revealed that the octahedral cation has a greater effect than the tetrahedral cation [45,47]. The peak found at 857-700 cm^{-1} in the Raman spectra of Fe-$CoAl_2O_4$ ceramics has been identified as the Al-O-Fe stretching vibration in the octahedron. This explains why octahedral cations have a larger influence on the wavenumber of the $A1^{3+}$ mode compared to tetrahedral cations [40,42,43,46,47]. The peak in 1339-1123 cm^{-1} region in the Raman spectra of Fe-$CoAl_2O_4$ ceramics is attributed to the Co^{3+}/Al-O stretching vibration in the octahedral sites. This peak is generally observed when cobalt ions are in octahedral coordination with aluminum ions [40,45,47]. The peak at 1418 cm^{-1} in the Raman spectra of Fe-$CoAl_2O_4$ ceramics is generally attributed to the Fe^{3+}/Al-O stretching vibration in the octahedral sites. This peak is normally observed in samples containing iron ions in octahedral coordination with aluminum ions [41,46,47]. The peak at 1684 cm^{-1} in the Raman spectra of Fe-$CoAl_2O_4$ ceramics is generally attributed to the Co^{3+}/Al-O asymmetric stretching vibration in the octahedral sites. This peak is normally observed when cobalt ions are in octahedral coordination with aluminum ions [44-47]. Through FT-Raman spectroscopic study, it has been confirmed that Fe-$CoAl_2O_4$ inverse spinel phase has been formed.

FE-SEM studies: Annealing temperatures of 600, 700, 800, 900 and 1000 ºC have been shown to yield Fe-Co-Al_2O_4 samples of different morphologies, as illustrated in Fig. 5.

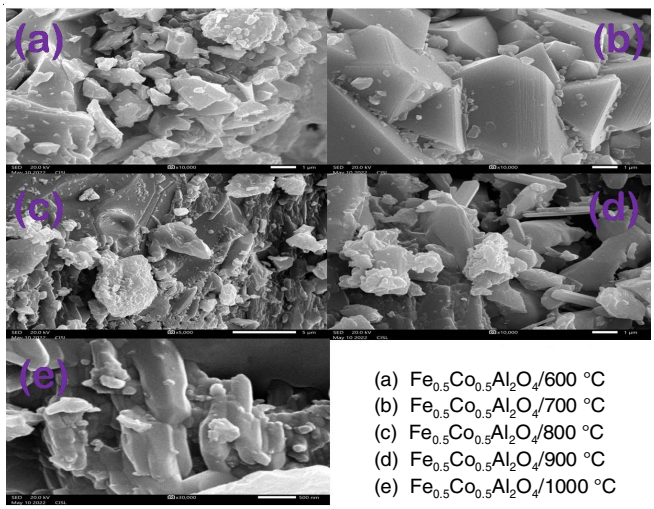

Fig. 5. FE-SEM images of Fe-Co-Al_2O_4 spinel aluminates annealed at 600, 700, 800, 900 and 1000 °C

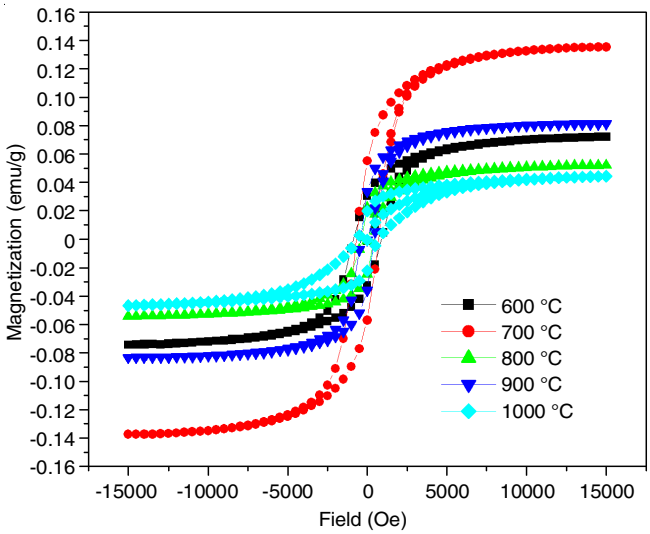

Fig. 6. Magnetization loop of Fe-Co-Al_2O_4 spinel aluminates annealed at 600, 700, 800, 900 and 1000 °C

Increasing annealing temperatures (600, 700, 800, 900 and 1000 ºC) of Fe-Co-Al_2O_4 powders leads to decreasing grain size and increasing agglomeration. For lower annealing temperatures (600, 700, 800 ºC), the particles are uniform in shape and size ranging from 20 to 100 nm, while for higher temperatures (900 and 1000 ºC), the particles become more irregularly shaped and range from 18.76 to 24.95 nm [16,37]. High resolution scanning electron microscopy shows that the nanoparticles are spherical in shape with some groups present in aggregation of spheres. This structure is further confirmed by X-ray diffraction, which confirms that these particles are spherical and present in an aggregated form.

VSM analysis of magnetic properties: VSM measurements were performed at different temperatures to study the changes in magnetic properties with temperature as shown in the Fig. 6. This analysis of Fe-Co-Al_2O_4 is a technique used to measure magnetic properties such as saturation magnetization (M_s), retentivity (M_r), coercivity (H_c), magnetic moment (μ_B), remnant ratio ($R = M_r/M_s$) and anisotropy constant (K). This analysis provides information about the magnetic characteristics of a material and allows comparison between different samples. The high coercivity value is indicative of hard ferrimagnetic materials because it indicates more resistance to external magnetic fields (Table-2). This means that the material has a stronger magnetization than other materials with a lower coercivity value [48]. The samples that were annealed at 600, 800, 900 and 1000 ºC have lower saturation magnetization values because these temperatures are not as effective at optimizing the magnetic properties of the material when compared to a temperature of 700 ºC. At lower temperatures, atoms are less able to move and re-orient themselves, resulting in weaker magnets with lower saturation magnetization values. The maximum value of M_s obtained for Fe-Co-Al_2O_4 sintered at 900 ºC was 30.6 emu/g, which is in agreement with samples annealed at 1000 ºC [49]. The higher saturation magnetization values obtained for samples annealed at 700 ºC and 900 ºC may be attributed to the multi-domain nature of their crystallites (Fig. 7). A multi-domain crystallite structure allows for improved magnetic moment ordering, which enables better magnetization performance in Fe-Co-Al_2O_4. This is because the higher magnetization can be better sustained by the crystallinity of the structure [50]. The increased magnetization capacity of Fe-Co-Al_2O_4 has numerous technological applications, due to the improved magnetization performance at higher annealing temperatures. Optimizing the M_s values at different annealing temperatures could potentially lead to further advancements and better performance in magnetic storage devices and other electromagnetism applications [51]. Factors such as grain size, lattice constant and strain can all affect the M_s values and thus the magnetization performance of Fe-Co-Al_2O_4. By researching these factors, it is possible to gain insight into the intrinsic properties that influence the M_s values and as a result, improve magnetization performance [39]. The increase in annealing temperature affects the coercivity, magnetic moment and Remnant ratio values of Fe-Co-Al_2O_4 samples (Fig. 8). At lower

TABLE-2
MAGNETIC PARAMETERS OF $Fe_{0.5}Co_{0.5}Al_2O_4$

Sample	M_s (emu/g)	M_r (emu/g)	H_c (Oe)	μ_B Tesla	R	K (J/m^3)
$Fe_{0.5}Co_{0.5}Al_2O_4$/600 °C	73.112×10^{-3}	31.366×10^{-3}	873.02	0.0041	0.4290	66.48
$Fe_{0.5}Co_{0.5}Al_2O_4$/700 °C	0.13635	56.084×10^{-3}	698.58	0.0070	0.4113	99.22
$Fe_{0.5}Co_{0.5}Al_2O_4$/800 °C	53.033×10^{-3}	23.293×10^{-3}	391.75	0.0029	0.4392	21.64
$Fe_{0.5}Co_{0.5}Al_2O_4$/900 °C	82.198×10^{-3}	34.664×10^{-3}	423.07	0.0046	0.4217	36.22
$Fe_{0.5}Co_{0.5}Al_2O_4$/1000 °C	45.421×10^{-3}	20.758×10^{-3}	698.66	0.0025	0.4570	33.05

Saturation magnetization (M_s), retentivity (M_r), coercivity (H_c), magnetic moment (μ_B), remnant ratio ($R=M_r/M_s$), anisotropy constant (K) and energy product (E_p)

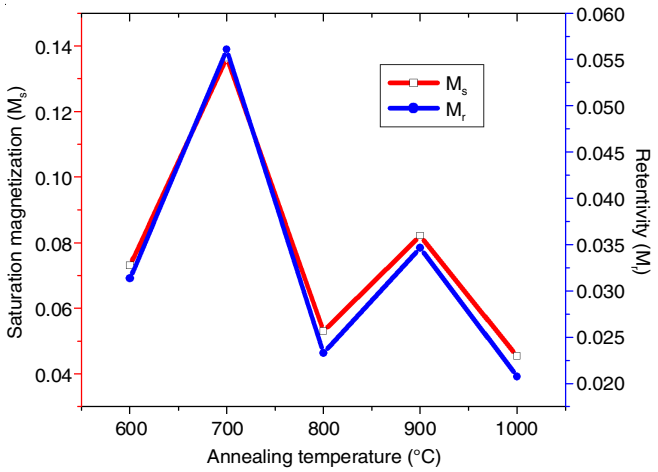

Fig. 7. Illustrates the relation between saturation magnetization and retentivity

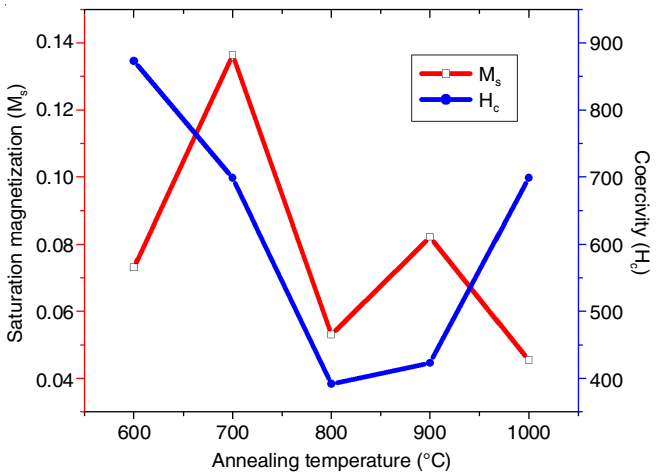

Fig. 8. Illustrates the relation between saturation magnetization and coercivity

temperatures, atoms are less able to move and reorient themselves, resulting in weaker magnetization with smaller coercivity, magnetic moment and Remnant ratio values. At higher temperatures, more atoms move and reorient themselves, resulting in a stronger magnetization with larger coercivity, magnetic moment and Remnant ratio values. This explains why these values increase or decrease with annealing temperature [52-57].

Conclusion

This work focused on the effects of increasing annealing temperatures on Fe-Co-Al_2O_4 spinel aluminates. It was found that higher temperatures resulted in an increase in the diffraction peaks, crystallite size and lattice constant up to 900 ºC, followed by a decrease due to increased diffusion of atoms and ions. The annealing temperature of Fe-Co-Al_2O_4 samples has a significant effect on their magnetic properties. At lower temperatures, the atoms are less able to move and reorient themselves, resulting in weaker magnetization with smaller coercivity, magnetic moment and Remnant ratio values. At higher temperatures, more atoms move and reorient themselves, resulting in a stronger magnetization with larger coercivity, magnetic moment and Remnant ratio values.

ACKNOWLEDGEMENTS

The authors gratefully acknowledge the research lab and library facilities provided by St. Joseph's College of Arts and Science (Autonomous), Cuddalore, India.

CONFLICT OF INTEREST

The authors declare that there is no conflict of interests regarding the publication of this article.

REFERENCES

1. G. Pilania, V. Kocevski, J.A. Valdez, C.R. Kreller and B.P. Uberuaga, *Commun. Mater.*, **1**, 84 (2020); https://doi.org/10.1038/s43246-020-00082-2
2. D.P. Dutta and G. Sharma, *Mater. Sci. Eng. B*, **176**, 177 (2011); https://doi.org/10.1016/j.mseb.2010.10.018
3. D. Dwibedi, C. Murugesan, M. Leskes and P. Barpanda, *Mater. Res. Bull.*, **98**, 219 (2018); https://doi.org/10.1016/j.materresbull.2017.10.010
4. F. Tielens, M. Calatayud, R. Franco, J.M. Recio, J. Pérez-Ramírez and C. Minot, *J. Phys. Chem. B*, **110**, 988 (2006); https://doi.org/10.1021/jp0533751
5. S. Deka, *Dalton Trans.*, **52**, 839 (2023); https://doi.org/10.1039/D2DT02733J
6. R. Sagayaraj, S. Aravazhi, P. Praveen and G. Chandrasekaran, *J. Mater. Sci. Mater. Electron.*, **29**, 2151 (2018); https://doi.org/10.1007/s10854-017-8127-4
7. E.K. Fodjo, K.M. Gabriel, B.Y. Serge, D. Li, C. Kong and A. Trokourey, *Chem. Cent. J.*, **11**, 58 (2017); https://doi.org/10.1186/s13065-017-0288-y
8. R. Sagayaraj, S. Aravazhi and G. Chandrasekaran, *J. Supercond. Nov. Magn.*, **31**, 3379 (2018); https://doi.org/10.1007/s10948-018-4593-z
9. C. Simon, A. Blösser, M. Eckardt, H. Kurz, B. Weber, M. Zobel and R. Marschall, *Z. Anorg. Allg. Chem.*, **647**, 2061 (2021); https://doi.org/10.1002/zaac.202100190
10. C.M. Álvarez-Docio, R. Portela, J.J. Reinosa, F. Rubio-Marcos, L. Pascual and J.F. Fernández, *Catalysts*, **10**, 406 (2020); https://doi.org/10.3390/catal10040406
11. M. Hao, P. Gao, W. Liu, B. Fang, J. Liang, T. Zhang, Y. Ding, H. Zhang and F. Wang, *Ceram. Int.*, **47**, 4722 (2021); https://doi.org/10.1016/j.ceramint.2020.10.041
12. Y. Tang, C. Wu, Y. Song, Y. Zheng and K. Zhao, *Ceram. Int.*, **44**, 1019 (2018); https://doi.org/10.1016/j.ceramint.2017.10.038
13. T. Gholami, M. Salavati-Niasari and S. Varshoy, *Int. J. Hydrogen Energy*, **41**, 9418 (2016); https://doi.org/10.1016/j.ijhydene.2016.03.144
14. C.M. Álvarez-Docio, J.J. Reinosa, A. del Campo and J.F. Fernández, *Dyes Pigments*, **137**, 1 (2017); https://doi.org/10.1016/j.dyepig.2016.09.061
15. H. Gao, H. Yang, S. Wang, D. Li, F. Wang, L. Fang, L. Lei, Y. Xiao and G. Yang, *J. Sol-Gel Sci. Technol.*, **86**, 206 (2018); https://doi.org/10.1007/s10971-018-4609-y
16. X. Peng, J. Cheng, J. Yuan, N. Jin, J. Kang, Y. Hou and Q. Zhang, *Adv. Appl. Ceramics*, **117**, 303 (2017); https://doi.org/10.1080/17436753.2017.1410941
17. T. Nakane, T. Naka, K. Sato, M. Taguchi, M. Nakayama, T. Mitsui, A. Matsushita and T. Chikyow, *Dalton Trans.*, **44**, 997 (2015); https://doi.org/10.1039/C4DT01599A
18. W. Zhang, J. Li, F. Zhong, G. Wu, H. Jiang, W. Zhang and Q. Liu, *J. Asian Ceramic Soc.*, **10**, 33 (2022); https://doi.org/10.1080/21870764.2021.2004727
19. A.K. Adak, S.K. Saha and P. Pramanik, *J. Mater. Sci. Lett.*, **16**, 234 (1997); https://doi.org/10.1023/A:1018512025919
20. R.L. Stewart and R.C. Bradt, *J. Mater. Sci.*, **15**, 67 (1980); https://doi.org/10.1007/BF00552428

21. X. Guo, P. Yin, K. Kanamori, K. Nakanishi and H. Yang, *J. Sol-Gel Sci. Technol.*, **88**, 114 (2018); https://doi.org/10.1007/s10971-018-4781-0
22. C. Feng, W.-J. Yin, J. Nie, X. Zu, M.N. Huda, S.-H. Wei, M.M. Al-Jassim, J.A. Turner and Y. Yan, *J. Appl. Phys.*, **111**, 093723 (2012); https://doi.org/10.1063/1.4716025
23. M. Raghasudha, D. Ravinder and P. Veerasomaiah, *Adv. Mater. Phys. Chem.*, **3**, 89 (2013); https://doi.org/10.4236/ampc.2013.32014
24. S.P. Waghmare, D.M. Borikar and K.G. Rewatkar, *Mater. Today Proc.*, **4**, 11866 (2017); https://doi.org/10.1016/j.matpr.2017.09.105
25. Y.M. Yakovlev, E.V. Rubalikaya and N. Lapovok, *Soviet Physics-Solid State*, **10**, 2301 (1969).
26. L. Ji, J. Lin and H.C. Zeng, *J. Phys. Chem. B*, **104**, 1783 (2000); https://doi.org/10.1021/jp993400l
27. S. Jayasree, A. Manikandan, A.M. Uduman Mohideen, C. Barathiraja and S.A. Antony, *Adv. Sci. Eng. Med.*, **7**, 672 (2015); https://doi.org/10.1166/asem.2015.1750
28. X. Zhao, L. Zhang, P. Xiong, W. Ma, N. Qian and W. Lu, *Micropor. Mesopor. Mater.*, **201**, 91 (2015); https://doi.org/10.1016/j.micromeso.2014.09.030
29. S. Salem, *Mater. Lett.*, **139**, 498 (2015); https://doi.org/10.1016/j.matlet.2014.10.118
30. Y. Song, Y.L. Zheng, Y.F. Tang and H.B. Yang, *Mater. Sci. Forum*, **898**, 1935 (2017); https://doi.org/10.4028/www.scientific.net/MSF.898.1935
31. T. Wu, S. Sun, J. Song, S. Xi, Y. Du, B. Chen, W.A. Sasangka, H. Liao, C.L. Gan, G.G. Scherer, L. Zeng, H. Wang, H. Li, A. Grimaud and Z.J. Xu, *Nat. Catal.*, **2**, 763 (2019); https://doi.org/10.1038/s41929-019-0325-4
32. D. El-Said Bakeer, *Appl. Phys., A Mater. Sci. Process.*, **126**, 443 (2020); https://doi.org/10.1007/s00339-020-03625-z
33. T. Nakane, S. Ishii, T. Uchikoshi and T. Naka, *J. Am. Ceram. Soc.*, **106**, 2317 (2023); https://doi.org/10.1111/jace.18915
34. A. Walsh, Y. Yan, M. AlJassim and S. Wei, *J. Phys. Chem. C*, **112**, 12044 (2008); https://doi.org/10.1021/jp711566k
35. N. Abbas, N. Rubab, N. Sadiq, S. Manzoor, M.I. Khan, J. Fernandez-Garcia, I. Barbosa-Aragao, M. Tariq, Z. Akhtar and G. Yasmin, *Water*, **12**, 2285 (2020); https://doi.org/10.3390/w12082285
36. A. Zhang, B. Mu, Z. Luo and A. Wang, *Dyes Pigments*, **139**, 473 (2017); https://doi.org/10.1016/j.dyepig.2016.12.055
37. H. Irfan, M. Racik K and S. Anand, *J. Asian Ceramic Soc.*, **6**, 54 (2018); https://doi.org/10.1080/21870764.2018.1439606
38. N.B. Granados, E. Yi, R. Laine and O.J.R. Baena, *Materia*, **20**, 580 (2015); https://doi.org/10.1590/S1517-707620150003.0059
39. R. Sagayaraj, S. Aravazhi and G. Chandrasekaran, *J. Inorg. Organomet. Polym. Mater.*, **29**, 2252 (2019); https://doi.org/10.1007/s10904-019-01183-3
40. T. Yu, Z.X. Shen, Y. Shi and J. Ding, *J. Phys. Condens. Matter*, **14**, L613 (2002); https://doi.org/10.1088/0953-8984/14/37/101
41. V. D'Ippolito, G.B. Andreozzi, D. Bersani and P.P. Lottici, *J. Raman Spectrosc.*, **46**, 1255 (2015); https://doi.org/10.1002/jrs.4764
42. C.M. Álvarez-Docio, J.J. Reinosa, A. Del Campo and J.F. Fernández, *J. Alloys Compd.*, **779**, 244 (2019); https://doi.org/10.1016/j.jallcom.2018.11.263
43. O.N. Shebanova and P. Lazor, *J. Solid State Chem.*, **174**, 424 (2003); https://doi.org/10.1016/S0022-4596(03)00294-9
44. M. Yamanaka and M. Ishii, *Phys. Chem. Miner.*, **13**, 156 (1986); https://doi.org/10.1007/BF00308157
45. M. Bouchard and A. Gambardella, *J. Raman Spectrosc.*, **41**, 1477 (2010); https://doi.org/10.1002/jrs.2645
46. B. Pathak, A. Yadav, P. Choudhary, M. Varshney and A. Mishra, *AIP Conf. Proc.*, **2100**, 020175 (2019); https://doi.org/10.1063/1.5098729
47. H. Shirai, Y. Morioka and I. Nakagawa, *J. Phys. Soc. Jpn.*, **51**, 592 (1982); https://doi.org/10.1143/JPSJ.51.592
48. R. Sagayaraj, S. Aravazhi, C. Selva kumar, S. Senthil kumar and G. Chandrasekaran, *SN Appl. Sci.*, **1**, 271 (2019); https://doi.org/10.1007/s42452-019-0244-7
49. R. Sagayaraj, T. Dhineshkumar, S. Aravazhi, G. Chandrasekaran, A. Prakash, D. Jayarajan and S. Sebastian, *Chem. Phys. Lett.*, **759**, 137944 (2020); https://doi.org/10.1016/j.cplett.2020.137944
50. R. Sagayaraj, S. Aravazhi and G. Chandrasekaran, *Appl. Phys., A Mater. Sci. Process.*, **127**, 502 (2021); https://doi.org/10.1007/s00339-021-04653-z
51. R. Sagayaraj, S. Aravazhi and G. Chandrasekaran, *Int. Nano Lett.*, **11**, 307 (2021); https://doi.org/10.1007/s40089-021-00343-z
52. R. Sagayaraj, *Int. Nano Lett.*, **12**, 345 (2022); https://doi.org/10.1007/s40089-022-00368-y
53. J. Subhashini, A.C. Ferdinand and R. Sagayaraj, *Chemistry Africa*, **5**, 1387 (2022); https://doi.org/10.1007/s42250-022-00438-w
54. A. Prakash, R. Sagayaraj, D. Jayarajan, S. Aravazhi, G. Chandrasekaran and R. Nithya, *Asian J. Chem.*, **34**, 2288 (2022); https://doi.org/10.14233/ajchem.2022.23840
55. A. Prakash, R. Sagayaraj, D. Jayarajan, S. Aravazhi, S. Sebastian, S. Sylvestre and C. Nyanga, *Chemistry Africa*, **5**, (2022); https://doi.org/10.1007/s42250-022-00570-7
56. R. Sagayaraj and S. Sebastian, *Appl. Phys., A Mater. Sci. Process.*, **129**, 98 (2023); https://doi.org/10.1007/s00339-022-06370-7
57. D. Jayarajan, R. Sagayaraj, S. Silvan, S. Sebastian, R. Nithya and S. Sujeetha, *Chemistry Africa*, **6**, (2023); https://doi.org/10.1007/s42250-023-00615-5